Marquette University

e-Publications@Marquette

Chemistry Faculty Research and Publications   Chemistry, Department of

1-1-2010

Anion Exchange Kinetics of Nanodimensional Layered Metal Hydroxides: Use of Isoconversional Analysis

Stephen Majoni
Marquette University

Jeanne Hossenlopp
Marquette University, jeanne.hossenlopp@marquette.edu

Anion Exchange Kinetics of Nanodimensional Layered Metal Hydroxides: Use of Isoconversional Analysis
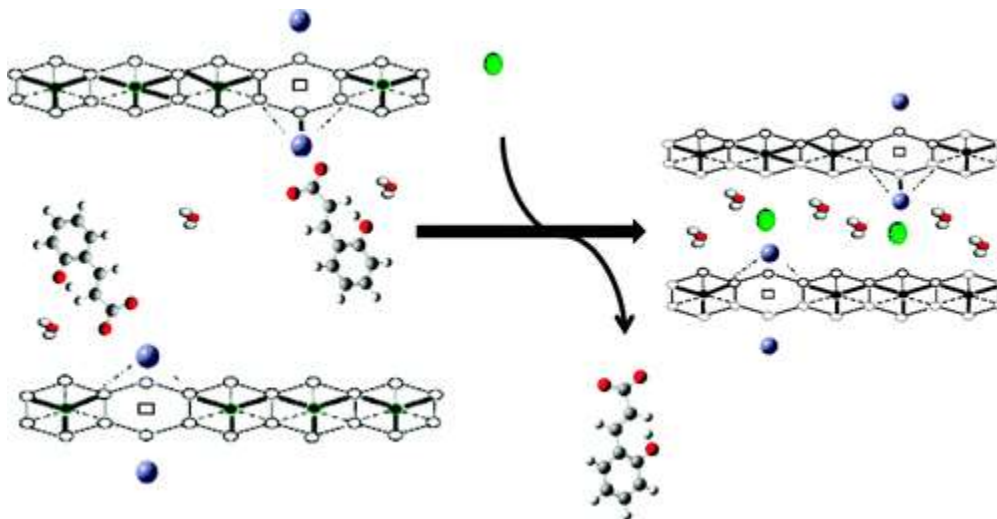
Stephen Majoni

Department of Chemistry, Marquette University, Milwaukee, WI

Jeanne M. Hossenlopp

Department of Chemistry, Marquette University, Milwaukee, WI

Abstract

Anion exchange reactions of nanodimensional layered metal hydroxide compounds are utilized to create materials with targeted physical and chemical properties and also as a means for controlled release of intercalated anions. The kinetics of this important class of reaction are generally characterized by model-based approaches. In this work, a different approach based on isothermal, isoconversional analysis was utilized to determine effective activation energies with respect to extent of reaction. Two different layered metal hydroxide materials were chosen for reaction with chloride anions, using a temperature range of 30−60 °C. The concentrations of anions released into solution and the changes in polycrystalline solid phases were evaluated using model-based (Avrami-Erofe'ev nucleation−growth model) and model-free (integral isoconversional) methods. The results demonstrate the utility of the isoconversional approach for identifying when fitting to a single model is not appropriate, particularly for characterizing the temperature dependence of the reaction kinetics.

1 Introduction

Layered metal hydroxides with exchangeable interlayer anions can be utilized to provide nanodimensional structures with tunable physical and chemical properties. This has resulted in these materials being used in flame retardadation,[1,2] ion-exchange, magnetism, and catalysis,[3-6] and as hosts for drugs, herbicides, and plant regulators.[7-10] Examples of these materials include layered double hydroxides (LDHs) $[M^{2+}_{1-x}M^{3+}_x (OH)_2]A^{n-}_{x/n} \cdot yH_2O$, hydroxy double salts (HDSs) $[(M^{2+}_{1-x}Me^{2+}_{1+x})(OH)_{3(1-y)/n}]A^{n-}_{(1+3y)/n} \cdot mH_2O$ where M^{2+} and Me^{2+} represent different divalent metal ions, and layered hydroxy salts (LHSs)

containing a single divalent metal ion. In all these materials A^{n-} is an exchangeable charge compensating anion of charge n which controls the interlayer space. The LDH layers have a brucite {Mg (OH)$_2$} type structure in which metal ions are surrounded by six hydroxide ions in an approximately octahedral geometry.[11] HDSs form similar structures, in some cases with unoccupied metal ion sites in the metal hydroxide layer, and tetrahedrally coordinated metal ions situated above and below the vacant sites.[12] Anion exchange reactions of layered metal hydroxides are useful for creating materials with optimal physicochemical properties for targeted applications, making the characterization of exchange kinetics of practical interest. In addition, understanding the factors that control release of functional anions from these structures is important in designing hosts for storage and triggered release.[7] Perhaps the most widely utilized approach for evaluating kinetics of this class of reactions has been the use of the Avrami-Erofe'ev nucleation−growth model.[13,14] In this model, the extent of reaction (α) is scaled from zero at the start of the reaction to one at the end, and depends upon the rate constant, k, and a coefficient, n, as shown in eq 1.

$$a(t) = 1 - e^{[-(kt)^n]} \qquad (1)$$

The coefficient n potentially contains information about the mechanism of the reaction and is often used to evaluate whether the reaction rate is controlled by diffusion or by nucleation and provides information on the dimension of growth.[15] eq 1 can be linearized by taking the natural logarithms twice obtaining eq 2.

$$\ln[-\ln(1 - \alpha)] = n\ln(t) + n\ln(k) \qquad (2)$$

The double-logarithmic plot of ln [−ln (1 − α)] as a function of ln t gives a linear plot in which the value of n is obtained from the slope and the value of k is evaluated from the intercept. Although double-logarithmic plots have been used since the 1950s,[16] they were made popular by Sharp and Hancock in 1972.[17] For reactions with different mechanisms, the double-logarithmic plots will have different slopes making it easy to distinguish reactions occurring via different mechanisms.[18] The Avrami-Erofe'ev model has been applied successfully to a wide range of reactions which includes crystallization

3

and phase transformations in glasses and alloys, metal hydrogenation reactions,[19] crystallization and growth of polymers,[20] and in anion exchange reactions of layered materials.[15,21,22]

However, this model-based approach is of limited use in cases where there are structural changes occurring during the exchange process. Although periods with different mechanisms can be distinguished in a double-logarithmic plot, obtaining an effective activation energy that can be utilized to describe the temperature dependence over the entire course of the reaction becomes difficult.[18] The Avrami-Erofe'ev model works well in some cases but is not sufficient when the mechanism is not constant over the entire extent of reaction and generally is used to fit to the data in a limited range $0.15 < \alpha < 0.85$.[15,21] The reliability of the Arrhenius parameters obtained from these model fitting procedures is subject to the proper choice of the reaction model.[23,24]

A strategy utilized in thermal analysis studies to identify when fitting to a single model is not an appropriate strategy is to utilize isoconversional methods as proposed by Vyazovkin and Wight.[25] Isoconversional methods have been applied successfully in a variety of reactions and allow for the determination of effective activation energies (E_a) for reactions which involve multiple steps which may reflect more than one mechanistic contribution.[26,27] The determination of how E_a varies as a function of the extent of reaction (α), provides information about the changes in reaction mechanism and enables the investigation of reaction mechanisms.[26,28] When a single process is involved, the E_a is constant over the conversion range; changes in E_a as a function of extent of reaction reflect changing contributions of individual processes involved in the reaction. For isothermal processes, isoconversional methods can be divided into differential methods (eq 3) and integral method (eqs 4).[26,29]

$$\ln\frac{d\alpha}{dt} = \ln[Af(\alpha)] - \frac{E_a}{RT} \qquad (3)$$

$$\ln t = \ln\frac{g(\alpha)}{A} + \frac{E_a}{RT} \qquad (4)$$

In eqs 3 and 4, E_a, and α are as defined before, A is the pre-exponential factor, t is the time, T the temperature, R is the gas constant, $f(α)$ and $g(α)$ are the reaction model and the integral reaction model respectively. The isoconversional approach has been widely applied in the degradation kinetics of a variety of materials which include polymers and inorganic molecules, recently the approach has been extended to other reactions which include hydride formation in reactive plasmas.[30]

In this work, we report the use of isothermal, isoconversional analysis to examine the anion exchange kinetics of two model reactions which have been chosen to illustrate how the isoconversional approach can be exploited to identify when model-based approaches such as Avrami-Erofe'ev kinetics, are appropriate. The selected examples involve release of cinnamate or hydroxycinnamate anions from HDS and LHS structures via exchange with chloride anions. Isoconversional analysis is applied to evaluate the rate of anion release into solution as well as changes in solid state structure in order to derive effective activation energies that can be compared to global E_a values obtained from the Avrami-Erofe'ev model fitting method.

2 Experimental Methods

2.1 Materials

Copper nitrate trihydrate [$Cu(NO_3)_2 \cdot 3H_2O$] (98.0%) and copper acetate monohydrate [$Cu(C_2H_3O_2)_2 \cdot H_2O$] (98.0%) were obtained from Alfa Aesar, trans-cinnamic acid [$C_6H_5CHCHCO_2H$], and trans-*o*-hydroxycinnamic acid [*o*-$(OH)C_6H_4CHCHCO_2H$] (98%), were obtained from Sigma Aldrich Chemical Co. Sodium chloride (100%) and zinc oxide (100%) were obtained from J. T. Baker. Sodium hydroxide (pellets, 98%) was obtained from EMD Chemicals. All materials were used as supplied by manufacturer without further purification.
2.2 Synthesis of Hydroxy Double Salts and Layered Hydroxy Salts
Precursor layered hydroxy salts (LHSs) and hydroxy double salts (HDSs) were prepared according to literature methods.[21,31,32] Basic copper nitrate (BCN) was prepared via a titration method; a 0.4 M copper nitrate solution was slowly titrated, under continuous stirring, with a 0.1 M NaOH solution until the ratio Cu^{2+}: OH^- of 1:1.5 was

achieved. Zinc copper hydroxy acetate (ZC-Ac) was prepared by adding 0.41 g of ZnO to 1.00 g of $Cu(CH_3COO)_2 \cdot H_2O$ in 10 mL of deionized (DI) water with vigorous stirring at room temperature. The resultant precipitates were filtered, washed several times with DI water, and dried at room temperature.

Copper hydroxy-*o*-hydroxycinnamate (C-*o*-HCn) and zinc copper hydroxy cinnamate (ZC-Cn) were prepared by anion exchange with the conditions for exchange being optimized for each material. The structures of the *o*-HCn and Cn anions used in this study are shown in Figure 1. To improve solubility in water, the acids (*o*-hydroxycinnamic acid and cinnamic acid) were reacted with an equimolar amount of NaOH in enough deionized water to produce the desired concentration for complete exchange of the precursor anion without observable degradation of the layered material. 20.0 g of BCN was mixed with 1000 cm^3 of 0.08 M *o*-hydroxycinnamate (*o*-HCn) solution at room temperature for 48 h with frequent stirring. The sample was filtered and the exchange reaction repeated twice with fresh *o*-HCn solutions in order to get complete exchange to form the C-*o*-HCn product. 20.0 g of ZC-Ac was mixed with 1000 cm^3 of 1.0 M cinnamate (Cn) and allowed to react at room temperature, with frequent stirring, for 8 h to produce the ZC-Cn product; longer reaction times led to degradation of the layered metal hydroxide. Elemental analysis of precursor and product layered metal hydroxides was performed by Huffman Laboratories, Colorado, using atomic emission spectroscopy interfaced with inductively coupled plasma (AES-ICP) for determination of metals.
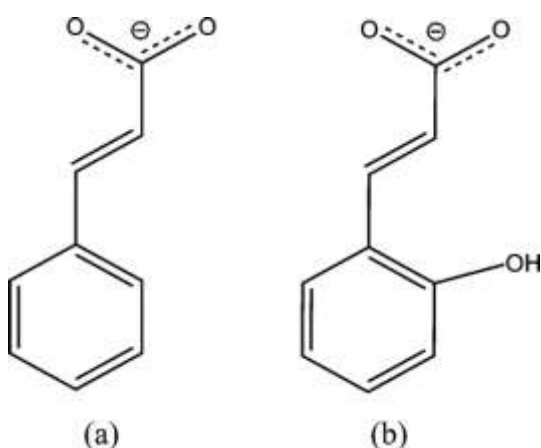

Figure 1. Structure of the anions used in this study: (a) cinnamate (Cn), (b) *o*-hydroxycinnamate (*o*-HCn).

2.2.1 Exchange Kinetics

The replacement of Cn or *o*-HCn anions by chloride ions as guest anions was investigated in the temperature range 30 to 60 °C. The exchange reactions were performed in a shaking water bath with a temperature stability of ±0.2 °C and shaking speed of 300 strokes per minute. Multiple reaction samples were prepared by mixing 0.15 g of C-*o*-HCn or ZC-Cn with 15 mL of 1.0 M sodium chloride; samples were continuously agitated in the water bath for a specified time period. After the specified time period, the reaction was quenched by filtration followed by washing of the residue several times with DI water. Solid samples were allowed to dry in air at room temperature prior to analysis. The concentration of released anions at specific time periods was monitored by UV−vis analysis on a Perkin-Elmer Lambda 35 UV−vis Spectrophotometer using quartz cuvettes with a path length of 1 cm. Representative UV−vis spectra are shown in Supporting Information Figure S1 and anions concentrations were monitored at the peak of the UV band (Cn, λ_{max} = 269 nm and *o*-HCn, λ_{max} = 270 nm). Calibration curves for calculating (hydroxy) cinnamate concentration in aqueous solutions were determined in the presence of sodium chloride concentrations identical to those used in the exchange reactions. The concentrations of released (hydroxy) cinnamate anions at time *t*, C_t, and the concentration at equilibrium, C_∞, were used to calculate the extent of reaction using eq 5.

$$\alpha = \frac{C_t}{C_\infty} \qquad (5)$$

For solid state transformation, the intensity of a given Bragg reflection was obtained by fitting the XRD peaks to a Gaussian or Lorentzian function. The disappearance of the (001) reflection of the host anion phase as well as the growth of the (001) reflection of chloride phase were monitored and the relative intensities of the host phase were used to calculate the extent of reaction for the decay of the host phase (α_{host}) at time (*t*) based on eq 6.

$$\alpha_{\text{host}(t)} = \left[\frac{1 - \left(\dfrac{I_{h(t)}}{I_{g(t)} + I_{h(t)}} \right)}{1 - \left(\dfrac{I_{h(\infty)}}{I_{g(\infty)} + I_{h(\infty)}} \right)} \right] \quad (6)$$

In eq $\underline{6}$, $I_{h(t)}$ is the intensity of a given Bragg reflection of the host anion at time t, $I_{g(t)}$ is the intensity of a given Bragg reflection of the guest anion at time t, $I_{h(\infty)}$ is the equilibrium intensity of the Bragg reflection of the host anion (determined at equilibrium) and $I_{g(\infty)}$ is the equilibrium intensity of the Bragg reflection of the guest anion (determined at equilibrium).

2.3 FTIR, Thermogravimetric Analysis and Powder X-ray Diffraction of Solids

Fourier transform infrared (FTIR) spectra of the layered materials were obtained on a Perkin-Elmer Spectrum 100 FT-IR spectrometer operated at a 2 cm⁻¹ resolution in the 4000−650 cm⁻¹ spectral range; 16 scans were averaged. The FTIR spectra were recorded using a single reflection ATR accessory with a ZnSe prism (PIKE MIRacle, from PIKE technology). Powder X-ray diffraction (PXRD) measurements were recorded on a Rigaku Miniflex II diffractometer using Cu Kα (λ =1.54 Å) radiation source at 30 kV and 15 mA. The patterns were recorded in the 2θ range of 2.0°−45.0°; data acquisition was performed using a step size of 0.0167° per second. The powder samples were pressed in to the trough of glass sample holders, the diffractometer was calibrated using a silicon reference material (RSRP-43275G: manufactured by Rigaku Corporation). Thermogravimetric analysis (TGA) was performed on a Netzsch TG 209 F1, TGA instrument. Samples with a weight of 10.0 ± 0.2 mg were placed into aluminum oxide crucibles and heated under a constant flow of nitrogen at a heating rate of 20 °C min⁻¹ between 40 and 800 °C.

2.4 Chain Length Calculation

The size of the nitrate anion and the chain length of Cn and *o*-HCn anions were calculated utilizing the Gaussian 98 program[33] and

carried out at the DFT (B3LYP) level of theory with 6-311++G(d,p) basis set. The chain length was calculated as the interatomic distance between the carboxyl oxygen and the furthest hydrogen atom.

3 Results and Discussion

3.1 Characterization of Precursor LHS and HDS

PXRD results for BCN, which has been indexed as the synthetic monoclinic gerhardtite $Cu_2(OH)_3NO_3$, space group *P 2$_1$/m* (4), (PDF # 45−594),[34] are shown in Figure 2A. The formula of gerhardtite is in close agreement with the formula obtained from elemental analysis $\{Cu_{2.3}(OH)_{3.6}(NO_3)\}$, the elemental analysis results are shown in Table S1 in the Supporting Information. Figure 2A shows the PXRD patterns for BCN (lower panel) and its exchange product (upper panel). In both cases, the materials show intense *00 l* reflections which are equally spaced indicating that the structures are layered and possess high range ordering, at least to the third order in the *c* axis direction. The *001−003* Bragg reflections were used to calculate the basal spacing of BCN using the Bragg equation,[35] the obtained value of 6.94 ± 0.01 Å matches literature value of 6.81 Å.[36] Upon exchanging nitrate with *o*-HCn, new peaks appear at lower 2 θ values (*001−003*) giving an average *d*-spacing value of 16.813 ± 0.003 Å; this is an indication of the expansion of the interlayer space. The increase of the interlayer space, from 6.94 Å in BCN to 16.81 Å in C-*o*-HCn, is consistent with a smaller nitrate anion (1.95 Å) being replaced by a larger *o*-HCn anion (chain length = 8.63 Å). The *o*-HCn anions are either tilted or partially interdigitated within the metal hydroxide layers. The absence of nitrate ion reflections from the C-*o*-HCn trace indicates that the exchange was complete; this is consistent with elemental analysis results (Table S1 in the Supporting Information). The metal ion to anion ratios are consistent, within approximately 10%, for a nearly 1:1 exchange.
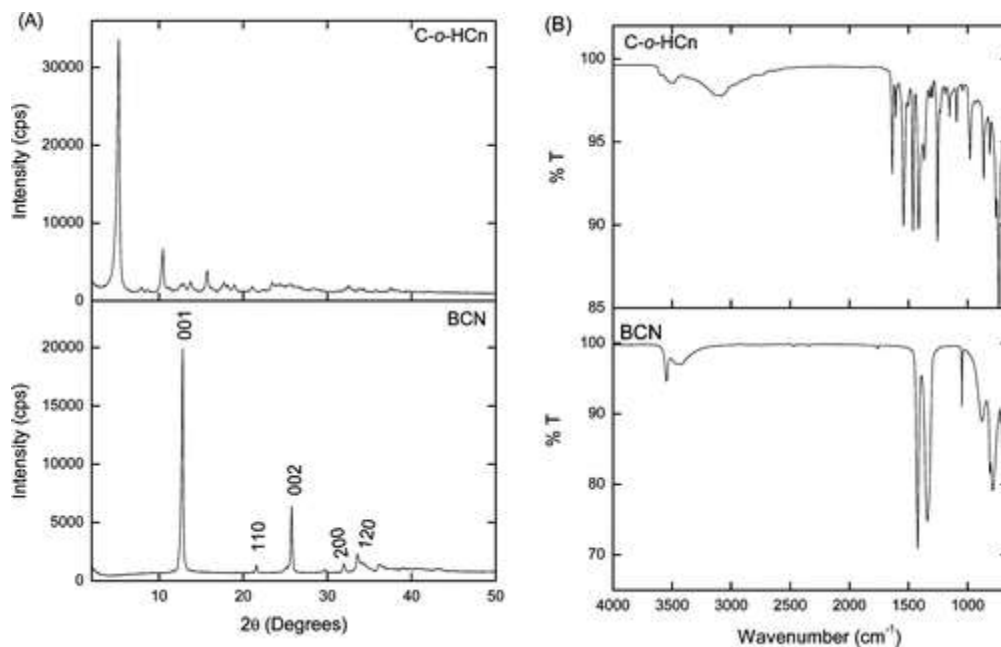
Figure 2. (A) PXRD profiles for BCN and C-*o*-HCn and (B) FTIR spectra for BCN and C-o-HCn.

FTIR spectra of BCN (lower panel) and C-*o*-HCn (upper panel) are shown in Figure 2B. Vibrational frequencies of BCN are in agreement with those obtained by other workers and have been assigned as follows; 1049 cm^{-1}, N−O stretching (v_2); 1338 cm^{-1}, O-NO$_2$ symmetric stretch (v_1); 1425 cm^{-1}, O-NO$_2$ asymmetric stretch (v_4).[36,37] The presence of two O-NO$_2$ peaks is consistent with vibrations of coordinated nitrate groups of C_{2v} symmetry. Coordination of the nitrate group to the matrix copper ion through one of the oxygen atoms reduces the symmetry of the nitrate ion from D_{3h} in free nitrate to C_{2v} resulting in splitting of the doubly degenerate NO$_2$ stretch (v_3, 1360−1380 cm^{-1}) in free nitrate.[37]

A set of new peaks appear in the exchange product corresponding to the presence of *o*-HCn in the gallery and the nitrate vibrational peaks disappeared, indicating complete exchange which is in agreement with PXRD results and elemental analysis results. The new peaks appear at 1639 cm^{-1} (C=C bond vibration of the α,β-unsaturated carboxylate group), 1540 cm^{-1} and 1417 cm^{-1} (v_{asym} C=O and v_{sym} C=O, respectively). There is extensive hydrogen bonding in C-*o*-HCn as indicated by the appearance of broad peaks and the disappearance of the sharp peak in the OH stretching region

10

$(3650-3000 \text{ cm}^{-1})$. Thermogravimetric analysis (Figure S2) and elemental analysis results (Table S1), provided as Supporting Information, demonstrate that the BCN precursor does not have a significant amount of intercalated water, whereas C-*o*-HCn does contain some associated water molecules which may reside within the interlayer space. The appearance of broad absorption peaks in C-*o*-HCn may be due to the presence of interlayer water molecules which formed hydrogen bonds with free layer hydroxyl groups or *o*-HCn molecules. Broad absorption bands in the OH stretching region have been shown to disappear with hydrous - anhydrous transformation, with the appearance of sharp absorption bands around 3600 cm^{-1}.[38]

ZC-Ac prepared in this work is layered and possesses high range ordering in the *c* direction as shown in the lower panel of Figure 3A; the PXRD profile show intense *00l (l* = 1 to 3) Bragg reflections which are equally spaced. The interlayer distance of 9.43 ± 0.03 Å obtained for ZC-Ac is comparable to literature values (9.3 Å and 9.46 Å) reported for material prepared using the same method.[21,32] The formula for ZC-Ac ($ZnCu_{2.8}(OH)_{5.3}(Ac)_{1.7} \cdot 2.6 \, H_2O$), obtained from elemental analysis data (Table S1) and TGA results (Figure S3), presented in Supporting Information, indicate that ZC-Ac has a significant amount of intercalated water molecules. When the acetate group in ZC-Ac was replaced with Cn ion, a shift of the Bragg reflections to lower 2 θ values was observed indicating expansion of the interlayer space, the interlayer distance increased to 20.21 ± 0.09 Å. The increase in the basal spacing is consistent with a smaller ion (acetate ion chain length = 2.53 Å) being replaced by a larger anion (Cn chain length = 8.62 Å) and with the cinnamate anions adopting a close to bilayer orientation.
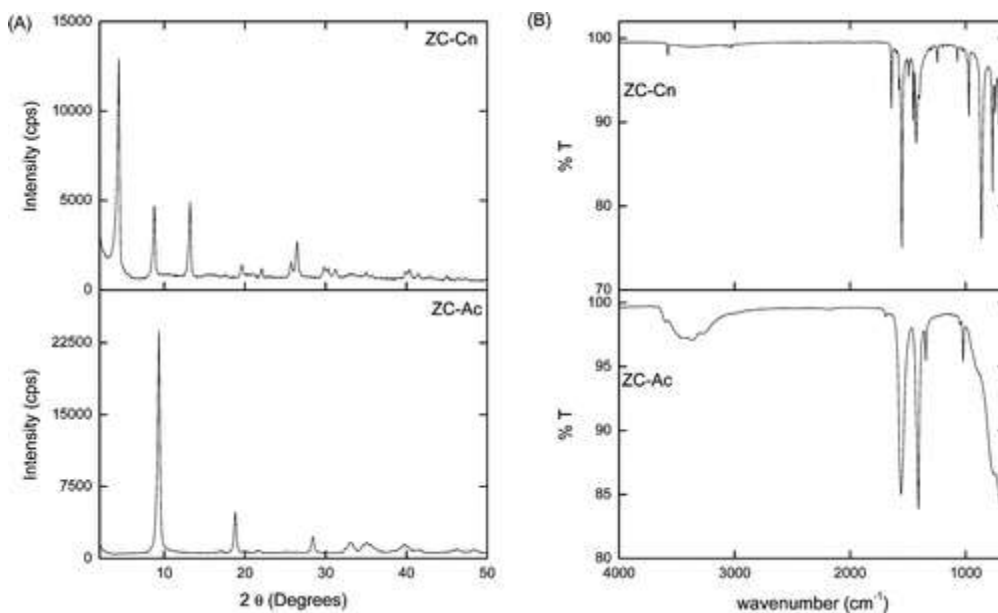
Figure 3. (A) PXRD profiles for ZC-Ac and ZC-Cn. (B) FTIR spectra for ZC-Ac and ZC-Cn.

IR spectra presented in Figure 3B shows that peaks due to C=O vibrations of acetate ion in ZC-Ac (υ_{asym} = 1563 cm^{-1} and υ_{sym} =1410 cm^{-1}) were replaced by a series of peaks due to Cn vibrations (1642 cm^{-1}, C=C bond vibration of the ɑ,β-unsaturated carboxylate group; 1551 cm^{-1}, υ_{asym} C=O and 1428 cm^{-1}, υ_{sym} C=O)-indicating complete replacement of acetate ions with Cn ions. ZC-Ac has a broad peak centered around 3400 cm^{-1} which is due to O−H stretch of hydrogen bonded water and/or layer hydroxyl groups. Upon exchanging acetate with Cn, the broad hydroxyl band in ZC-Ac was replaced by a single sharp peak at 3577 cm^{-1} in ZC-Cn; this is consistent with losing water of intercalation as the acetate ion was replaced by Cn resulting resulting in the layer hydroxyl groups being free,[38] consistent with elemental analysis data, Table S1, and TGA data, Figure S2, provided in Supporting Information.

3.2 Kinetic Analysis

Anionic exchange reactions in clays are generally viewed as topotactic, with overall structural integrity maintained during the reaction, although the nature of the lamellar structure and the anions involved can result in a dissolution-reprecipitation mechanism.[39] The reactions may involve multiple steps which include:

- Transport of the guest ions in the bulk solution and their subsequent diffusion across the liquid film surrounding the lamellar compound;
- Diffusion of the guest within the interlayer space to completely fill the space;
- Chemical reaction at exchange sites within the layers;
- Diffusion of the host anion (displaced from the layers) in the interlayer space and its subsequent diffusion in the bulk solution away from the lamellar compound.

3.3 Kinetic Analysis in C-o-HCn

The PXRD analysis of the solid samples obtained during the exchange reaction provides insight into the transformation of both the guest phase and the host phase during the reaction. Selections of traces at different time periods for all the temperatures are shown in Figure 4. In addition to reflections from *o*-HCn, new reflections that increase in intensity with time appear at higher 2θ values. These reflections are assigned to layered products containing intercalated Cl⁻ ions. There are two Cl⁻ phases, with the one with higher intensity (major phase) being indexed as monoclinic botallackite $\{Cu_2(OH)_3Cl\}$, space group *P2₁/m* (11), PDF # 58−520, and the minor phase (lower intensity) was indexed as monoclinic clinoatacamite $\{Cu_2Cl(OH)_3\}$, space group *P2₁/n* (14), PDF # 50−1559.[34] The botallackite phase has a *001* peak at 2θ = 15.5° corresponding to a *d*-spacing of 5.74 ± 0.049 Å which is in close agreement with reported value for $Cu_2(OH)_3Cl$ of 5.726 Å.[40] The clinoatacamite phase *011* peak at 16.2°, corresponding to a *d*-spacing of 5.29 ± 0.03 Å, is in agreement with reported value of 5.47 Å.[41] The assignments have been confirmed by examining higher angle data as shown in Figure S4 in Supporting Information. In Figure 4, the *o*-HCn phase is marked by closed diamonds, botallackite phase by closed circles and the clinoatacamite phase by closed squares. As expected for release kinetics, the intensity of the Cl⁻ phases (guest anion) increase with time while the *o*-HCn phase intensity (host anion) decrease relative to the Cl⁻ phase. The reaction does not go to completion since the Bragg reflections from the *o*-HCn phase are still observed at equilibrium (t_∞).
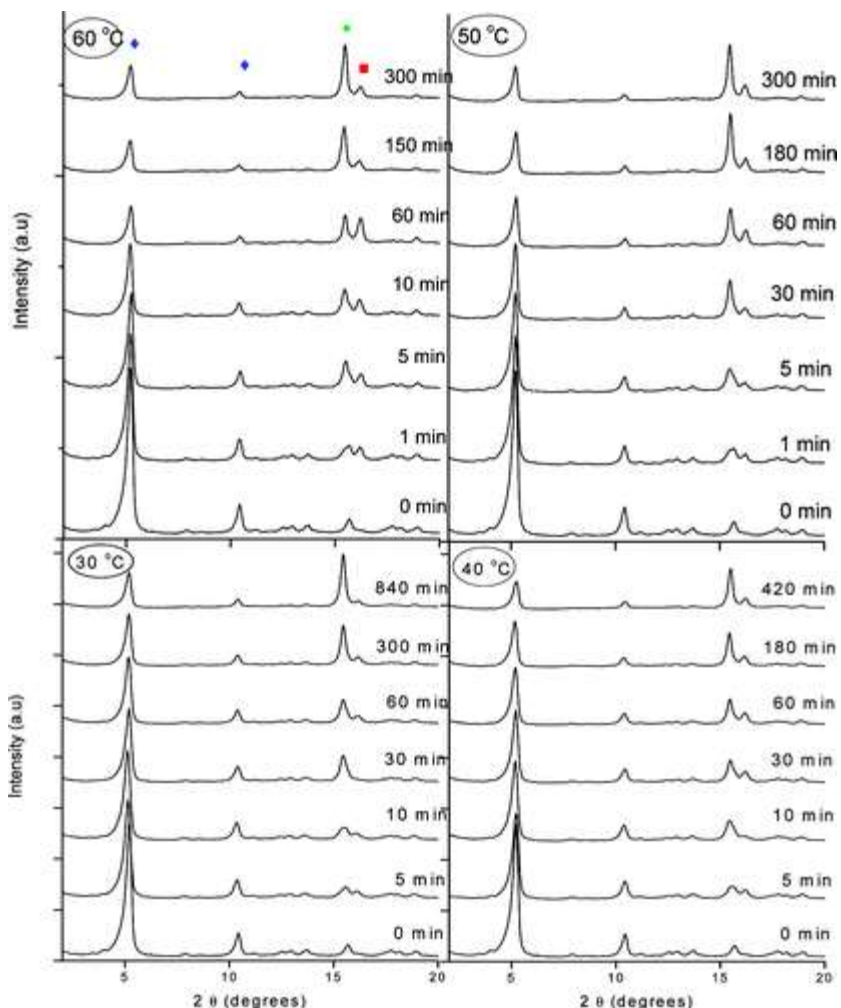
Figure 4. PXRD profile for solid samples collected at different times and at different temperatures for the C-*o*-HCn/Cl⁻ reaction. The *o*-HCn phase is represented by closed diamonds, botallackite phase by closed circles and the clinoatacamite phase by closed squares.

The intercalation mechanism in layered materials has been shown to involve staging in materials with flexible layers such as graphite intercalation compounds (GIC), this phenomenon of staging involves filling of every n^{th} layer in the nth stage compound.[42] Staging has been postulated to be a mechanism for lowering of the activation energy for intercalation and exchange reactions.[43] Although the layers in clays are too rigid for staging to occur,[44,45] the phenomenon has, however, been observed in a few LDH systems where only second stage compounds have been formed; in LDHs staging depends on the intercalated anions and the composition of the layers.[43,46-49] Second-stage compounds contain alternating interlayers occupied by different

anions. Only first-order staging was observed in this study since the XRD profiles did not show series of 00*l* basal reflections at 2 θ positions corresponding to the sum of the interlayer space of the starting material and the fully exchanged product (for second order stage compound) as shown in Figure 4. The absence of higher order staging may indicate that the interaction between the layers and the initial anion are strong as compared to the layer-guest interaction resulting in a small reduction in the E_a being attained through staging.[49]

The extent of reaction as a function of time plots obtained from solid state transformations at different temperatures are shown in Figure 5A. The sum of peak heights of the 001 botallackite and the 011 clinoatacamite reflections was used to determine the product $I_{g(t)}$ values. The extent of reaction versus time data were fit to the Avrami-Erofe'ev nucleation−growth model (eq 1); the model provided good fit within the range of α of 0.15−0.85 as has been observed for other intercalation reactions in layered materials.[21,50] Within this specified range of α, the model fits the obtained experimental data as shown from the corresponding double-logarithmic plots in Figure 5B, where straight lines were obtained with R^2 values ranging from 0.986 to 0.996. The double-logarithmic plots shown in Figure 5B are almost parallel with an *n* value of ~0.5 indicating that, for the temperature range used here, the mechanism is the same and is consistent with being diffusion controlled.[15] UV−vis spectroscopy was used to determine the accumulated amounts of *o*-HCn in the filtrate, and hence the amount of host anion released into solution. Since the Avrami-Erofe'ev model has been successfully applied to liquid phase UV−vis and NMR data of released anions,[7,21,51] it was also applied here to the solution data in order to determine whether the model provides a good description of the release process. The release profiles are shown in Figure 6 and the corresponding double-logarithmic plots are presented in Supporting Information Figure S5. The double-logarithmic plots are linear for all the temperatures used here which is an indication that the Avrami-Erofe'ev model provides a good description of the liquid phase data within the range 0.15 < α < 0.85. The resulting fits are represented by solid lines in the profiles shown in Figure 6. Similar to the solid phase transformation results, the *n* values are again consistent with a diffusion controlled process.

Calculated rate constants (k) and Avrami n coefficients are provided in Table 1 for the kinetics of solid state transformation and the anion release into solution.
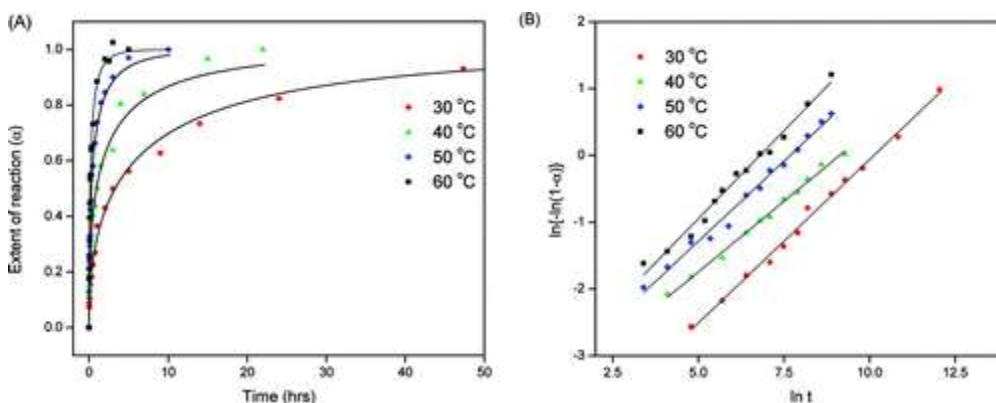

Figure 5. (A) Extent of reaction as a function of time and (B) corresponding double-logarithmic plots for the exchange reaction of Cl⁻ anion and C-*o*-HCn at various temperatures for solid state analysis: 60 °C (□), 50 °C (♦), 40 °C (▲), 30 °C (●), the extent of reaction data has been fitted to Avrami-Erofe'ev equation (solid lines).
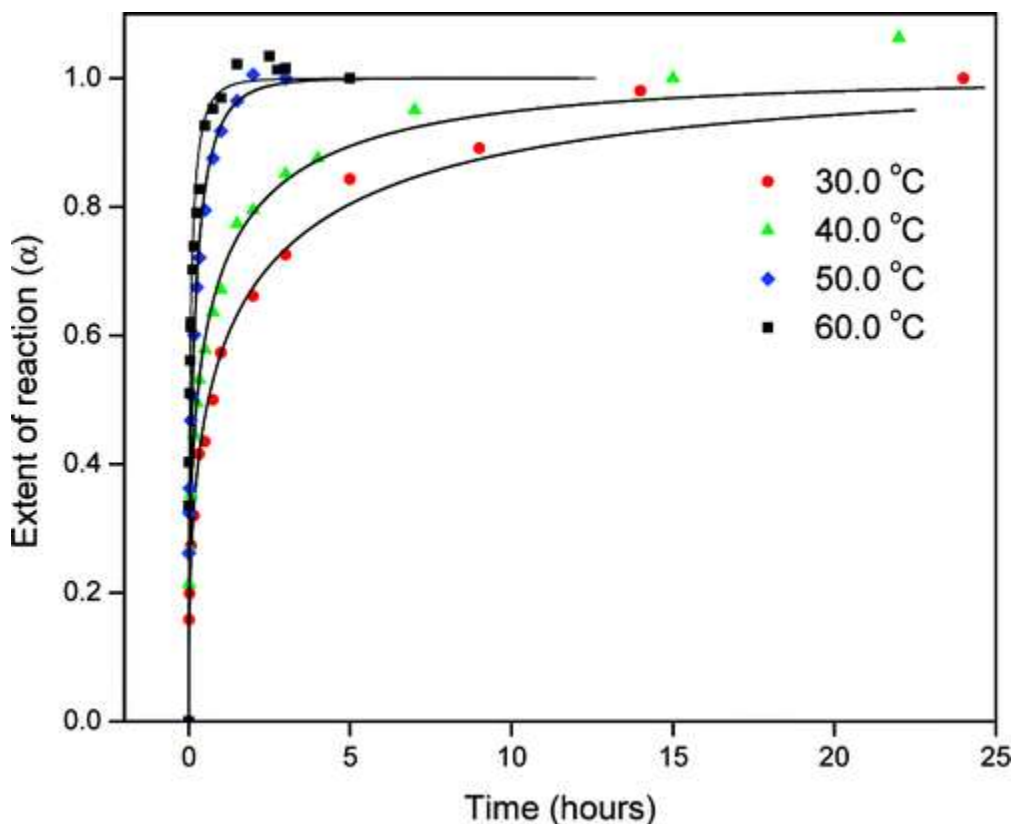
Figure 6. Extent of reaction as a function of time for the exchange reaction of C-*o*-HCn at various temperatures for solution analysis: 60 °C (□), 50 °C (♦), 40 °C (▲), 30 °C (●), the extent of reaction data has been fitted to Avrami-Erofe'ev equation.

Table 1. Summary of Solid State and Solution Analysis Kinetic Parameters Obtained from the Double-Logarithmic Plots Analysis for the Reaction of C-*o*-HCn at Different Temperatures

T (°C)	Solid state		Solution phase	
	n	k s⁻¹(×10⁻⁴)	*n*	k s⁻¹(×10⁻⁴)
	n	$k\,s^{-1}(\times 10^{-4})$	n	$k\,s^{-1}(\times 10^{-4})$
60.0	0.52 ± 0.02	11 ± 3	0.397 ± 0.006	29 ± 4
50.0	0.48 ± 0.01	4 ± 1	0.45 ± 0.02	16 ± 4
40.0	0.45 ± 0.01	1.3 ± 0.2	0.39 ± 0.06	4.3 ± 0.7
30.0	0.45 ± 0.01	0.4 ± 0.1	0.40 ± 0.01	1.6 ± 0.4

As observed in Table 1, the rate constants obtained for anion release into solution are three to four times larger than the corresponding rate constants for the solid state transformation. The differences between solution analysis and solid state transformation may indicate that the loss of the host anion and subsequent loss of coherent diffraction from the host phase occurs faster than the gain in coherent diffraction from the product phase. This has been observed in other systems and maybe due to the presence of an intermediate with poor crystallinity[52] or a delayed appearance of the guest phase which may be because a significant number of layers need to be filled with the guest to observe Bragg reflection from the guest phase. Since higher order staging was not observed in this study, the onset of the exchange reaction may then occur from the outermost layers, and parallel to the layers as observed in the intercalation of NH_3 into TaS_2[53] and deintercalation of mercury from TiS_2.[54] Johnsen et al.[55] observed a similar effect in the exchange reaction of chloride into carbonate-containing LDH. In cases such as these, mixed phases with different interlayer separations should be observed in XRD profiles.[56] The progressive increase in the number of layers occupied by the guest anions results in the growth of the guest phase and the decay of the host phase with time as observed in XRD profiles.

In our system, if the anion exchange reaction proceeds from layer-to-layer, with a smaller anion replacing a larger anion, then the rigid HDS layers are expected to collapse to the interlayer dimension of the guest phase when the majority of the host anions in the layers have been replaced. Unless the complete exchange within the individual layers is instantaneous, the growth of the guest phase and the decay of the host phase may be delayed relative to the time that host anions are observed being released into solution. Therefore, some of the C-*o*-HCn may be consumed and significant amount of *o*-HCn

released into solution without subsequent appearance of guest diffraction peaks.[49,57,58] Due to the ex situ analysis of the solid product, the decay of the host phase was referenced to the growth of the guest (chloride) phase in obtaining the extent of reaction as shown in eq 6. The rate of decay of the host phase and the growth of the guest phase are therefore interlinked to give the observed rate constants. The low rate of growth of the chloride phase due to factors indicated above will affect the extent of reaction values obtained, resulting in the observed lower rates of reaction compared to solution analysis.

The temperature dependence of the reaction was evaluated via Arrhenius plots shown in Supporting Information Figure S6. The value of the effective activation energy was 91 ± 3 kJ/mol for the solid phase transformation (Figure S6A of the Supporting Information). The Arrhenius plot for the anion release into solution, Figure S6B of the Supporting Information, resulted in an E_a of 84 ± 5 kJ/mol. These values are not significantly different indicating that the temperature dependence obtained from these two approaches is comparable. When the chemical reaction at the exchange sites is rapid, the transport process (by diffusion) then determines the overall rate of reaction. The Avrami n coefficient values obtained from analyzing both the solid materials and the solution phase released anion concentrations were, as noted previously, consistent with a diffusion-controlled mechanism. Diffusion-controlled processes have been shown to have varying E_a values depending on the nature of the reaction conditions. While the value for aqueous diffusion-controlled reactions of ions is low (~15 kJ mol^{-1}),[59] values for surface adsorption processes are reported to be as high as 30 kJ mol^{-1}.[60] During the sorption of 2,4-Dichlorophenoxyacetate on various clays, Haque et al.[61] observed E_a values ranging from 12−21 kJ mol^{-1}. Lv et al.[62] obtained two E_a values for the two-step removal of fluoride ions from solution using an LDH. The fast first step was considered to be diffusion controlled and had an E_a value of 37 kJmol^{-1}, while the second slower step, with an E_a value of 72 kJ mol^{-1}, was proposed to be controlled by the chemical reaction of F$^-$ with the LDH layers.[62] The E_a values for 2-dimensional (2-D) diffusion within the layers may be even higher, depending on the nature of the interlayer species and how densely packed the anions are. When the interlayer species are organic anions, the diffusion through the organic matrix can resemble diffusion through polymers

with E_a values ranging up to 100 kJ mol^{-1}, depending on the diffusing molecule.[63] In ion exchange reactions in lamellar compounds, Ragavan et al.[50] found an activation energy of 43 kJ mol^{-1} for the diffusion-controlled intercalation of 4-chlorophenoxyacetate and 53−62 kJ mol^{-1} for intercalation reactions presumed to be controlled by nucleation at the edge of the layers, based on the Avrami model results. The E_a values for processes controlled by reactions of the anions with the lamellar compounds have been shown to range from 30−70 kJ mol^{-1} depending on the nature and size of the guest anions, with larger anions having higher E_a values.[50,52,64] If our reaction is diffusion-controlled, as implied by the Avrami n values, then 2-D diffusion in the interlayer region would be the most likely rate determining factor. However, a mechanistic contribution from the exchange reaction cannot be ruled out.

While the Avrami model appears to fit the data with similar values of n obtained at the range of temperatures used here, it is clear from Figure 5 that fit is not perfect, particularly at higher conversions at 40 °C. Isoconversional analysis offers the advantage of being able to determine the variation of activation energy as a function of reaction progress; this provides information regarding how the reaction mechanism may change as a function of extent of reaction.[25] The results obtained from isoconversional analysis for solid state analysis and solution analysis are shown in Figure 7, parts A and B, respectively. The E_a values obtained for solid state data range from 87−96 kJ mol^{-1} and those for solution analysis range from 78−85 kJ mol^{-1}. The data shown in Figure 7 for both solid state and solution analysis reveal that, within experimental error, the E_a does not significantly change as a function of extent of reaction. This is an indication that the reaction can be described as proceeding via a single mechanism, consistent with fact that the Avrami n values did not vary significantly as a function of temperature for each data set. The E_a values obtained from the Avrami-Erofe'ev analysis lie within the range of values obtained using isoconversional method, indicating that in this case the model fitting approach provides reliable averaged global effective activation energy for the entire reaction. As noted above, the E_a values obtained are too high to be explained by diffusion of ions in solution alone, 2-D diffusion in a densely packed interlayer region may explain the high E_a values obtained here. In basic copper nitrate, the

interlayer anions are grafted onto the layers,[65] consistent with FTIR analysis discussed earlier. The *o*-HCn is therefore also expected to be bound to the layer and the observed E_a values are also consistent with a mechanism in which the rate is determined by the reaction at the exchange site. Since E_a does not vary as a function of extent of reaction, fitting the data to a single reaction model is appropriate but further work is necessary to better characterize the nature of the rate-determining process.
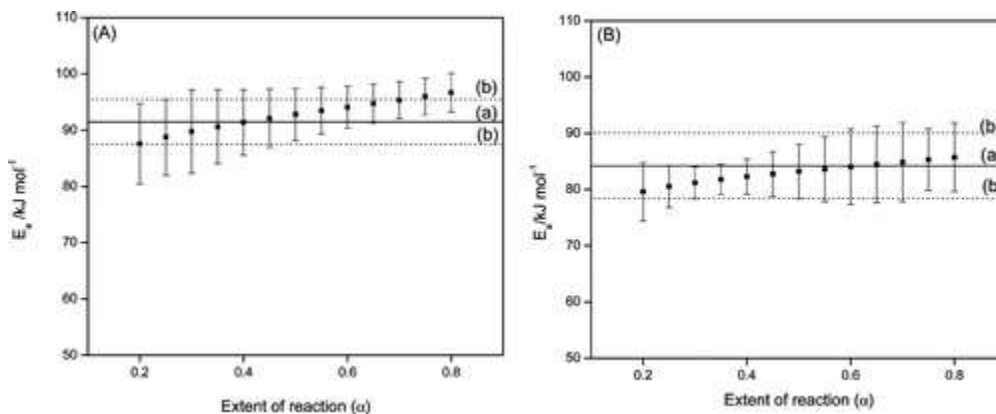
Figure 7. Variation of effective E_a with α for (A) solid state analysis and (B) Solution analysis. The solid line (a) represents the Arrhenius determined E_a together with the associated errors (broken lines, b).

3.4 Kinetic Analysis for ZC-Cn

The solid state transformation of both the guest and the host phases during the replacement of Cn by chloride in the ZC-Cn HDS host are shown in Figure 8, with the chloride phase indicated by an arrow. There is a small induction period observed at low temperatures (30 and 40 °C) as seen in Figure 8. Induction periods have been observed for other anion exchange reactions[48] and may be due to restructuring of the host layers which results in a delayed or slow release of the Cn anions and subsequent delayed crystallization and/or growth of the guest phase. During the induction period, the chloride phase is not observed for a period of up to 5 min at 30 °C, and then starts to grow slowly with Bragg reflections having very low intensities in samples obtained for reaction times less than 20 min. This effect is also observed in solution analysis where there was linear and slow increase in the concentration of released Cn in the first 30 min (Figure S7, in Supporting Information). Possibilities for the slow release of Cn

ions without corresponding growth of guest phase include (1) that there were Cn anions present on the edges of interlayer region of the material, or (2) that there where protonated Cn molecules adsorbed on the surface. Only trace amounts of Cn were released when the material was placed in DI water at 40 °C for 24 h without any sodium chloride present, much less than the amount released during the induction period. This suggests that the anions released during the induction period were ions on the edges of the lamellar compounds which were exchanged by chloride ions in solution. The chloride phase, which has been indexed as paratacamite, zincian (PDF # 50−1558),[34] has a first peak (*101*) at 2θ = 16.15° corresponding to a *d*-spacing of 5.47 ± 0.01which is in agreement with the literature value of 5.45 Å.[66] More detail concerning the phase assignment is found in Supporting Information Figure S8. Similar to the C-*o*-HCn system, only the first-stage compound was observed.
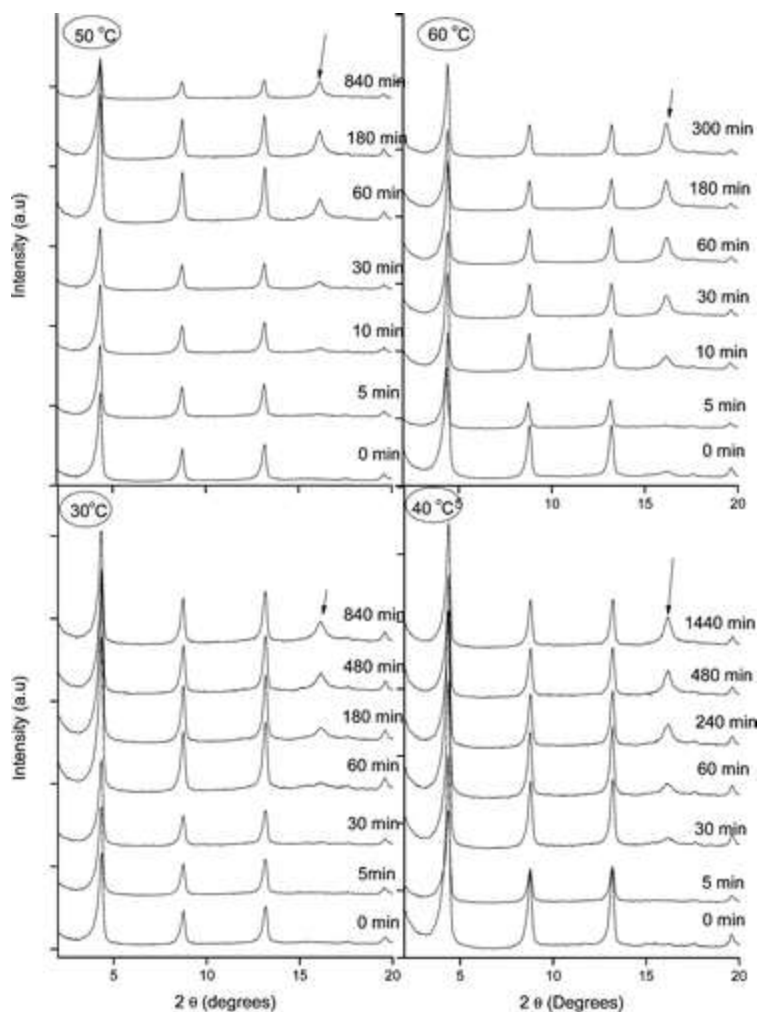
Figure 8. PXRD profile for solid samples collected at different times and different temperatures for the reaction of ZC-Cn with chloride anion. The chloride phase is indicated with an arrow.

The absolute extent of reaction for the exchange is low as indicated by the high intensity of the Cn phase in relation to the guest phase (chloride) at equilibrium. For anion exchange reactions, there are a number of factors which affect the affinity of the HDS layers for guest anion; these include layer-host anion interactions, layer-guest anion interactions, host anion-guest anion interactions within the interlayer space, and the solvation energies of both the host and guest anions. These factors could have resulted in a low equilibrium constant for the exchange reaction.

The extent of reaction versus time plot for solid state transformations at different temperatures are shown in Figure 9, the

data were again fit to the Avrami-Erofe'ev nucleation−growth model (solid line) using double-logarithmic plots (found in Supporting Information Figure S9A). Note that the double-logarithmic analysis required an offset in the lower temperature for t_o in order to take into account the induction period. While linear double-logarithmic plots were obtained, the Avrami-Erofe'ev model does not extrapolate to fit the induction region $\alpha < 0.15$ for the lower temperatures, as is evident in the insert in Figure 9. The Avrami exponent obtained in this analysis ranged from 0.6 to 0.9, indicating that for the temperatures 30 and 40 °C ($n \approx 0.6$) the reaction appears primarily diffusion controlled and for 50 and 60 °C ($n \approx 0.9$) there may be contributions from both diffusion and nucleation.[21] The rate constants obtained for both the solid state transformation and the solution analysis are not significantly different which may indicate that the solid state transformation has the same general kinetics as the release of anions into solution for $0.15 < \alpha < 1.0$. In this case, due to the induction period and the corresponding low initial release of Cn anions into solution, the loss of the host anions and subsequent loss of coherent diffraction from the host phase occurred at the same rate as the gain in coherent diffraction from the product phase.
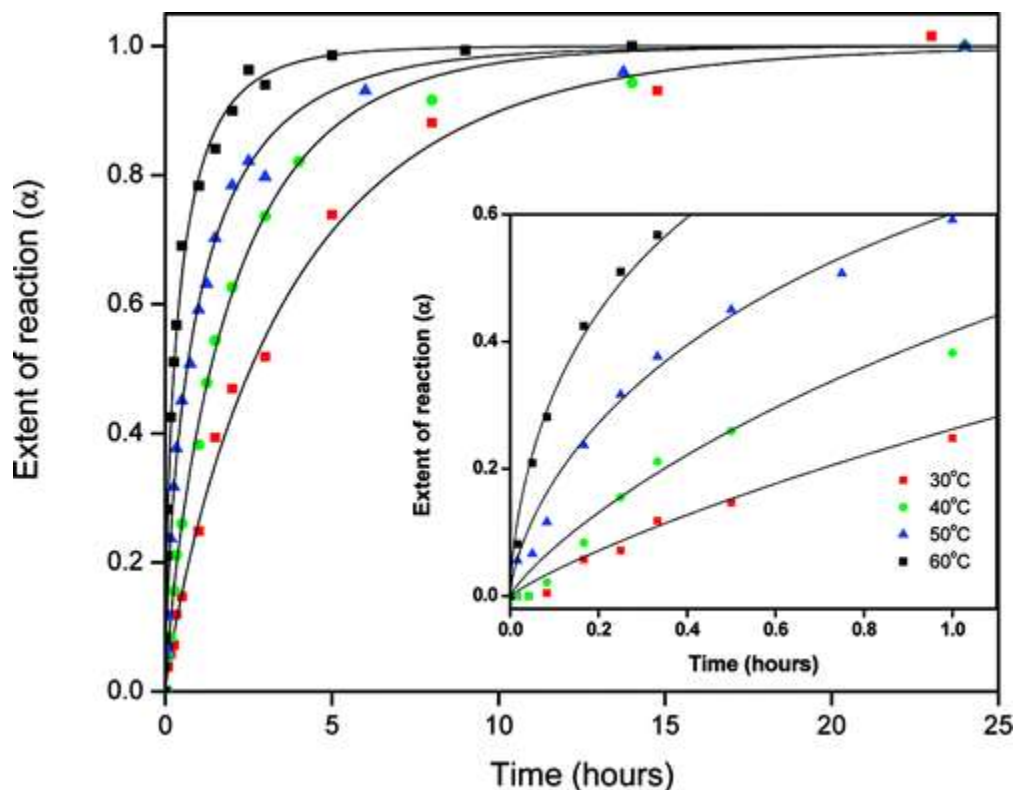
Figure 9. Release profile for the exchange reaction of Cl⁻ and ZC-Cn at various temperatures for solid state analysis: 60 °C (□), 50 °C (blue ▲), 40 °C (green ●), 30 °C (red □). The insert shows low time regime highlighting the induction period for 30 and 40 °C, note the induction is no longer present at higher temperatures.

The Avrami-Erofe'ev model was also applied to the solution data obtained from UV−vis spectroscopy. The release profiles are shown in Figure 10 (corresponding double-logarithmic plots are in Supporting Information Figure S9B). The Avrami exponents obtained ranged from 0.4 to 0.8; with a similar temperature dependent variation as observed in the solid phase data. The kinetic parameters obtained from double-logarithmic analysis are presented in Table 2. The effective activation energy for the release of Cn was obtained by using both model fitting methods and model free methods. The Arrhenius plots for the Avrami model data are shown in Figure S6C for solid state analysis and Figure S6D of the Supporting Information for solution analysis. For solid state transformation, the Avrami model led to activation energy of 58 ± 4 kJ/mol. The corresponding E_a for monitoring the anion release into solution was 45 ± 7 kJ/mol. These values obtained from both solid state and solution analysis are comparable; this is to be expected since the rate constants are not significantly different therefore the temperature dependence is not expected to be different.
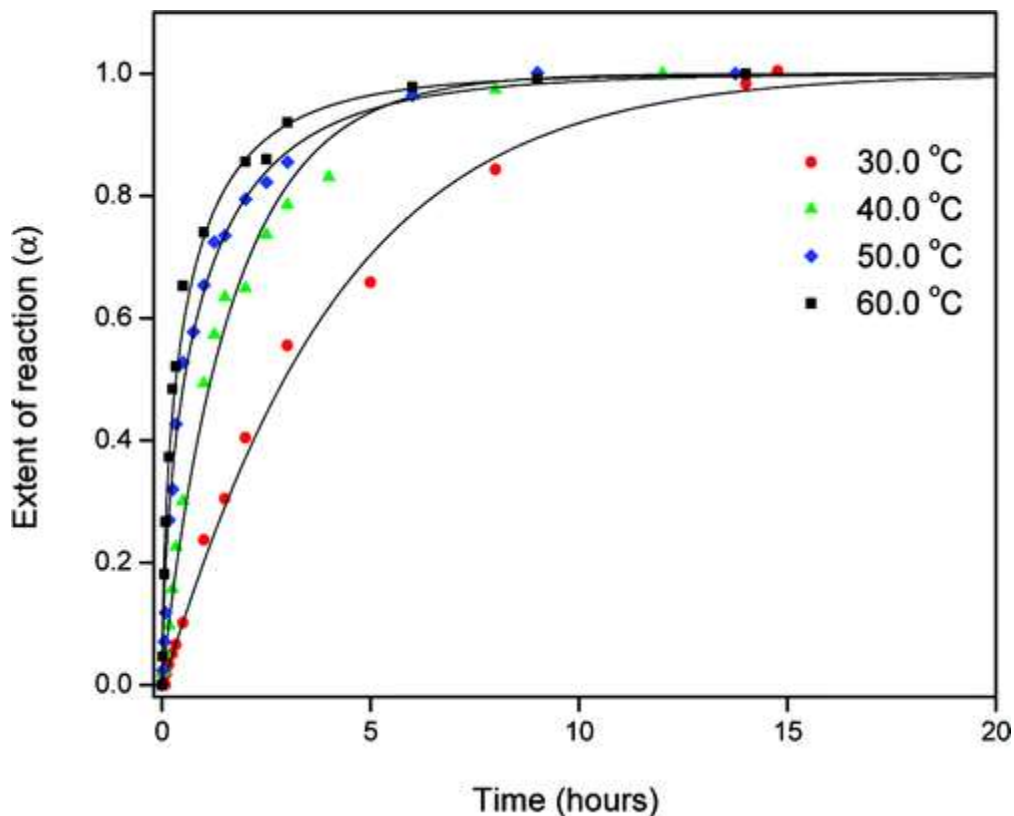
Figure 10. Extent of reaction as a function of time for the exchange reaction of Cl⁻ anion and ZC-Cn at various temperatures for solution analysis: 60 °C (□), 50 °C (♦), 40 °C (▼), 30 °C (●), data has been fitted to Avrami -Erofe'ev equation.

Table 2. Summary of Kinetic Parameters Obtained at Different Temperatures for the Reaction of ZC-Cn with Cl⁻

	Solid state		**Solution phase**	
***T* (°C)**	***n***	**k s⁻¹(×10⁻⁴)**	***n***	**k s⁻¹(×10⁻⁴)**
60.0	0.61 ± 0.02	6 ± 1	0.41 ± 0.01	4 ± 1
50.0	0.66 ± 0.02	2.4 ± 0.6	0.60 ± 0.02	2.9 ± 0.7
40.0	0.88 ± 0.01	1.3 ± 0.4	0.71 ± 0.02	1.7 ± 0.4
30.0	0.87 ± 0.01	0.7 ± 0.2	0.75 ± 0.02	0.7 ± 0.2

The isoconversional treatment of the solid state data shows a linear variation of E_a as a function of extent of reaction (Figure 11A). The E_a start at a value of 102 kJ mol⁻¹ at an extent of reaction of 0.05 and drops to 45 kJ mol⁻¹ at an extent of reaction of 0.8. There is also variation in the E_a with extent of reaction for solution data (Figure 11B); the E_a does not change significantly from extent of reaction of 0.05 up to 0.15 (83−80 kJ mol⁻¹) and then decreases linearly to 41 kJ mol⁻¹ at α = 0.8. The variation of E_a as a function of extent of reaction

is an indication that the reaction does not proceed via a single mechanism and the decrease in effective E_a may indicate that there is a decreasing contribution from an initial mechanistic step (or set of steps) with higher E_a. The obtained activation energy therefore cannot be assigned to a single process or interpreted in terms of the transition state theory.[23] There is a significant difference between solid state analysis and solution analysis at low extent of reaction (0.05 < α < 0.15), the E_a for solution analysis does not significantly change while the variation in effective activation energy for the solid state reaction is more pronounced. The solution phase analysis showed almost constant E_a at the early stage of reaction where there is release of Cn from the materials without corresponding growth of the chloride phase. This could be due to chemisorption/desorption of Cl^- and Cn ions on the edges of the interlayer space of the lamellar compound. After the initial chemisorption process at the edges, the exchange of interior (interlayer) Cn ions could result in increased rates of exchange and increased accumulation of released host anions and subsequent decay and growth of the host and guest anion phases respectively. In the ZC-HCn structure, the layers are positively charged with the charge being generated when a quarter of the octahedral sites in the copper hydroxide layers are vacant and Zn^{2+} ions occupy the tetrahedral sites on either side of the vacant octahedral site.[12] Therefore, there is electrostatic interaction between the layers and the interlayer anions. It has been observed in anion exchange in LDHs that the exchange and complete replacement of host anions with guest anion within the layers increase the rate of anion-exchange in the neighboring layers.[55] This has also been observed in intercalation reactions in TiS_2 where the intercalation of one layer results in the weakening of the neighboring layer reducing the E_a for intercalation.[67] If the reaction rate is controlled by anion exchange within the layers, then lowering of the effective E_a of exchange in the neighboring layers may result in the gradual lowering of E_a values for the reaction as the exchange proceeds. This may explain the trend observed in both the solution analysis and solid state analysis. Transition from a chemical-reaction-controlled process to a diffusion-controlled process cannot be ruled out since the E_a values obtained at high extent of reaction are in the range of diffusion controlled reactions. However, it is clear in this case that a single mechanism is inadequate to characterize the observed kinetics.
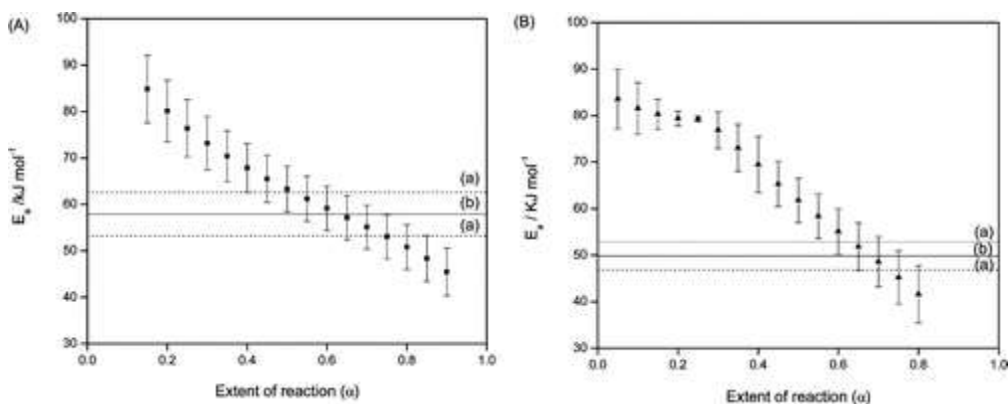
Figure 11. Plot of the variation of activation energy with the extent of reaction (α) for (A) solid state analysis and (B) Solution analysis. The solid line (b) represents the Arrhenius determined activation energy and broken lines (a) represent the associated errors.

Understanding the effect of the metal hydroxide layer structure in potentially controlling the observed kinetics is the subject of ongoing work in our laboratory, using the same host/guest anion combinations with different metal hydroxide layers. In addition, variations in host and/or guest anions in reactions involving the same metal hydroxide layer are also being explored.

4 Conclusions

Isoconversional analysis has been successfully applied, for the first time, to anion release kinetics in layered materials. The effective activation energies obtained from isoconversional analysis indicated that, for the C-*o*-HCn system, there is no variation in the mechanism of the reaction; the E_a values remained constant with respect to extent of reaction, within the limits of experimental uncertainty. The effective activation energies for replacement of *o*-HCn by chloride that were extracted from the isoconversional analysis ranged from 87−96 kJ mol^{-1} in solid state analysis and 78−85 kJ mol^{-1} for solution analysis and were found to be in agreement with those obtained from a global fit to the data using the Avrami-Erofe'ev model. In the second model system presented here, ZC-Cn reaction with chloride, there was a clear variation of the E_a with respect to extent of reaction indicating that there where changes in the reaction mechanism as the reaction progressed. The Avrami-Erofe'ev model, or any other single mechanism, is therefore inadequate for modeling the reaction kinetics, particularly for determining the effect of temperature over the entire

extent of reaction. Use of isothermal, isoconversional approaches is a convenient method for testing the applicability of the Avrami (or any other model-based) approach.

Acknowledgment

References

[1]Chigwada, G.; Kandare, E.; Wang, D. Y.; Majoni, S.; Mlambo, D.; Wilkie, C. A.; Hossenlopp, J. M. J. Nanosci. Nanotechnol. 2008, 8, 1927– 1936

[2]Majoni, S.; Su, S.; Hossenlopp, J. M. Polym. Degrad. Stab. 2010, 95, 1593– 1604

[3]Dutta, P. K.; Puri, M. J. Phys. Chem. 1989, 93, 376– 381

[4]Fujita, W.; Awaga, K. Inorg. Chem. 1996, 35, 1915– 1917

[5]Hayashi, H.; Hudson, M. J. J. Mater. Chem. 1995, 5, 781– 783

[6]Taibi, M.; Ammar, S.; Jouini, N.; Fievet, F.; Molinie, P.; Drillon, M. J. Mater. Chem. 2002, 12, 3238– 3244

[7]Khan, A. I.; Ragavan, A.; Fong, B.; Markland, C.; O'Brien, M.; Dunbar, T. G.; Williams, G. R.; O'Hare, D. Ind. Eng. Chem. Res. 2009, 48, 10196– 10205

[8]bin Hussein, M. Z.; Zainal, Z.; Yahaya, A. H.; Foo, D. W. V. J. Controlled Release 2002, 82, 417– 427

[9]Gu, Z.; Thomas, A. C.; Xu, Z. P.; Campbell, J. H.; Lu, G. Q. Chem. Mater. 2008, 20, 3715– 3722

[10]Hwang, S. H.; Han, Y. S.; Choy, J. H. Bull. Korean Chem. Soc. 2001, 22, 1019– 1022

[11]Miyata, S. Clays Clay Miner. 1983, 31, 305– 311

[12]Morioka, H.; Tagaya, H.; Karasu, M.; Kadokawa, J.; Chiba, K. Inorg. Chem. 1999, 38, 4211– 4216

[13]Avrami, M. J. Chem. Phys. 1940, 8, 212– 224

[14]Avrami, M. J. Chem. Phys. 1941, 9, 177– 184

[15]Francis, R. J.; O'Brien, S.; Fogg, A. M.; Halasyamani, P. S.; O'Hare, D.; Loiseau, T.; Ferey, G. J. Am. Chem. Soc. 1999, 121, 1002– 1015

[16]Young, D. A.Decomposition of Solids. In The International Encyclopedia of Physical Chemistry and Chemical Physics, 21st ed.; Tompkins, F. C., Ed.;Pergamon Press Ltd: Oxford, 1966. Vol 1.

[17]Hancock, J. D.; Sharp, J. H. J. Am. Chem. Soc. 1972, 55, 74– 77

[18]Millange, F.; Walton, R. I.; O'Hare, D. J.Mater.Chem. 2000, 10, 1713– 1720

[19]Saitoh, H.; Machida, A.; Katayama, Y.; Aoki, K. Appl. Phys. Lett. 2009, 94, 151915

[20]Sperling, L. H.; Introduction to Physical Polymer Science, 4th ed.; John Wiley & Sons: Hoboken, NJ, 2006; Chapter 6, pp 239– 323.

[21]Kandare, E.; Hossenlopp, J. M. J. Phys. Chem. B 2005, 109, 8469– 8475

[22]Khan, A. I.; O'Hare, D. J. Mater.Chem. 2002, 12, 3191– 3198

[23]Vyazovkin, S.; Wight, C. A. Annu. Rev. Phys. Chem. 1997, 48, 125– 149

[24]Vyazovkin, S. V.; Lesnikovich, A. I. Thermochim. Acta 1990, 165, 11– 15

[25]Vyazovkin, S.; Wight, C. A. Thermochim. Acta 1999, 340−341, 53− 68

[26]Vyazovkin, S. In The Handbook of Thermal Analysis & Calorimetry; Brown, M. E.; Gallagher, P. K., Eds.; Recent Advances, Techniques and Applications; Elsevier: Oxford, 2008; Vol. 5, pp 503− 538.

[27]Vyazovkin, S. Int. Rev. Phys. Chem. 2000, 19, 45− 60

[28]Vyazovkin, S.; Goryachko, V.; Bogdanova, V.; Guslev, V. Thermochim. Acta 1993, 215, 325− 328

[29]Budrugeac, P.; Homentcovschi, D.; Segal, E. J. Therm. Anal. Calorim. 2001, 63, 457− 463

[30]Quaas, M.; Wulff, H.; Ivanova, O.; Helm, C. A. Z. Kristallogr. 2009, 241− 246

[31]Biswick, T.; Jones, W.; Pacula, A.; Serwicka, E.; Podobinski, J. J. Solid State Chem. 2007, 180, 1171− 1179

[32]Rajamathi, J. T.; Britto, S.; Rajamathi, M. J. Chem. Sci. 2005, 117, 629− 633

[33]Gaussian 98, Revision A.11.4. Frisch, M. J.; Trucks, G. W.; Schlegel, H. B.; Scuseria, G. E.; Robb, M. A.; Cheeseman, J. R.; Zakrzewski, V. G.; Montgomery, J A. Jr.; Stratmann, R. E.; Burant, J. C.; Dapprich, S.; Millam, J. M.; Daniels, A. D.; Kudin, K. N.; Strain, M. C.; Farkas, O.; Tomasi, J.; Barone, V.; Cossi, M.; Cammi, R.; Mennucci, B.; Pomelli, C.; Adamo, C.; Clifford, S.; Ochterski, J.; Petersson, G. A.; Ayala, P. Y.; Cui, Q.; Morokuma, K.; Rega, N.; Salvador, P.; Dannenberg, J. J.; Malick, D. K.; Rabuck, A. D.; Raghavachari, K.; Foresman, J. B.; Cioslowski, J.; Ortiz, J. V.; Baboul, A. G.; Stefanov, B. B.; Liu, G.; Liashenko, A.; Piskorz, P.; Komaromi, I.; Gomperts, R.; Martin, R. L.; Fox, D. J.; Keith, T.; Al-Laham, M. A.; Peng, C. Y.; Nanayakkara, A.; Challacombe, M.; Gill, P. M. W.; Johnson, B.; Chen, W.; Wong, M. W.; Andres, J. L.; Gonzalez, C.; Head-Gordon, M.; Replogle, E. S.; Pople, J. A., Gaussian, Inc., Pittsburgh PA, 2002.

[34]Powder Diffraction File. Andrews, L. C.; Bernstein, L. R.; Foris, C. M.; McClune, W. F.; Rendle, D. F.; Rohrman, A. C.; Rotella, F. J.; Ryba, E.; Wallace, P. L. Alphabetical Indexes for Experimental Pattern. Set 1−59 International Centre for Diffraction Data, Inorganic Phases: Newtown Square, 2009.

[35]Pecharsky, V. K.; Zavalij, P. Y. Fundamentals of Powder Diffraction and Structural Characterization of Materials; Kluwer Academic Publishers: Boston, MA, 2001; Chapter 2, pp 100− 260.

[36]Pereira, D. C.; de Faria, D. L. A.; Constantino, V. R. L. J. Brazil. Chem. Soc. 2006, 17, 1651− 1657

[37]Addison, C. C.; Gatehouse, B. M. J. Chem. Soc. 1960, 613− 616

[38]Rabu, P.; Drillon, M.; Hornick, C. Analusis 2000, 28, 103− 108

[39]Prasanna, S. V.; Kamath, P. V. J. Colloid Interface Sci. 2009, 331, 439− 445

[40]Jimenez-Lopez, A.; Rodriguez-Castellon, E.; Olivera-Pastor, P.; Maireles-Torres, P.; Tomlinson, A. A. G.; Jones, D. J.; Roziere, J. J. Mater. Chem. 1993, 3, 303− 307

[41]Jambor, J. L.; Dutrizac, J. E.; Roberts, A. C.; Grice, J. D.; Szymanski, J. T. Can. Mineral. 1996, 34, 61− 72

[42]Baerlett, N.; McQuillan, B. W. In Intercalation Chemistry, Materials Science Series; Whittingham, M. S.; Jacobson, A. J., Eds.; Academic Press: New York, 1982; Chapter 2, pp 19− 98.

[43]Williams, G. R.; O'Hare, D. Chem. Mater. 2005, 17, 2632– 2640

[44]Solin, S. A. J. Mol. Catal. 1984, 27, 293– 303

[45]Solin, S. A. Annu. Rev. Mater. Sci. 1997, 27, 89– 115

[46]Fogg, A. M.; Dunn, J. S.; O'Hare, D. Chem. Mater. 1998, 10, 356– 360

[47]Iyi, N.; Kurashima, K.; Fujita, T. Chem. Mater. 2002, 14, 583– 589

[48]Williams, G. R.; Norquist, A. J.; O'Hare, D. Chem. Mater. 2004, 16, 975– 981

[49]Williams, G. R.; Fogg, A. M.; Sloan, J.; Taviot-Gueho, C.; O'Hare, D. Dalton Trans. 2007, 3499– 3506

[50]Ragavan, A.; Khan, A.; O'Hare, D. J. Mater. Chem. 2006, 16, 4155– 4159

[51]Miladinovic, Z.; Zakrzewska, J.; Kovacevic, B.; Bacic, G. Mater. Chem. Phys. 2007, 104, 384– 389

[52]Williams, G. R.; Dunbar, T. G.; Beer, A. J.; Fogg, A. M.; O'Hare, D. J. Mater. Chem. 2006, 16, 1222– 1230

[53]Mckelvy, M. J.; Sharma, R.; Glaunsinger, W. S. Solid State Ionics 1993, 63−5, 369– 377

[54]McKelvy, M.; Sidorov, M.; Marie, A.; Sharma, R.; Glaunsinger, W. Chem. Mater. 1994, 6, 2233– 2245

[55]Johnsen, R. E.; Krumeich, F.; Norby, P. J. Appl. Crystallogr. 2010, 43, 434– 447

[56]Evans, J. S. O.; Price, S. J.; Wong, H. V.; O'Hare, D. J. Am. Chem. Soc. 1998, 120, 10837– 10846

[57]Williams, G.; Khan, A.; O'Hare, D. In Layered Double Hydroxides: Structure and Bonding 119; Duan, X.; Evans, D. G., Eds; Springer: Berlin Heidelberg:, 2006; pp 161– 192.

[58]Taviot-Gueho, C.; Feng, Y.; Faour, A.; Leroux, F. Dalton Trans. 2010, 39, 5994– 6005

[59]Pilling, M. J.; Seakins, P. W. Reaction Kinetics; Oxford University Press: New York, 1995.

[60]Ho, Y. S.; Ng, J. C. Y.; Mckay, G. Sep. Purif. Methods 2000, 29, 189– 232

[61]Haque, R.; Lindstrom, F. T.; Freed, V. H.; Sexton, R. Environ. Sci. Technol. 1968, 2, 207– 211

[62]Lv, L.; He, J.; Wei, M.; Evans, D. G.; Zhou, Z. L. Water Res. 2007, 41, 1534– 1542

[63]ten Hulscher, T.; Cornelissen, G. Chemosphere 1996, 32, 609– 626

[64]Ragavan, A.; Khan, A. I.; O'Hare, D. J.Mater.Chem. 2006, 16, 602– 608

[65]Fujita, W.; Awaga, K.; Yokoyama, T. Inorg. Chem. 1997, 36, 196– 199

[66]Braithwaite, R. S. W.; Mereiter, K.; Paar, W. H.; Clark, A. M. Mineral. Mag. 2004, 68, 527– 539

[67]Acrivos, J. V. In Intercalated Layered Materials; Lévy, F., Ed.; D. Reidel Publishing Company: Dordrecht, 1979; Chapter 1, pp 33– 98.

Supporting Information

Supporting Information

for

Anion Exchange Kinetics of Nanodimensional Layered Metal Hydroxides: Use of Isoconversional Analysis

Stephen Majoni, Jeanne M. Hossenlopp*

Department of Chemistry

Marquette University, P.O. Box 1881

Milwaukee, WI 53201-1881

*Corresponding author. Tel.; +1 414 288 3537; fax: + 1 414 288 7066.

E-mail: Jeanne.hossenlopp@marquette.edu

CONTENTS

Table S1: Summary of elemental analysis data.

Compound	Elemental analysis: experimental (calculated)				
	% N	% Zn	% Cu	% H	% C
$Cu_{2.3}(OH)_{3.6}(NO_3)$	4.98(5.13)	0.00	52.56 (54.28)	1.34 (1.37)	< 0.03
$Cu_{2.0}(OH)_{2.9}(o\text{-}HCn)_{1.1}0\cdot6H_2O$	< 0.03	0.00	36.61 (35.64)	3.24 (3.25)	32.94 (32.66)
$ZnCu_{2.8}(OH)_{5.3}(Ac)_{1.7}\cdot2.6\ H_2O$	0.00	14.72 (14.15)	35.84 (34.44)	3.25 (3.39)	9.25 (8.90)
$ZnCu_{3.2}(OH)_{6.1}(Cn)_{2.4}$	0.00	8.81 (9.06)	27.8 (28.57)	3.00 (3.08)	35.14 (36.11)
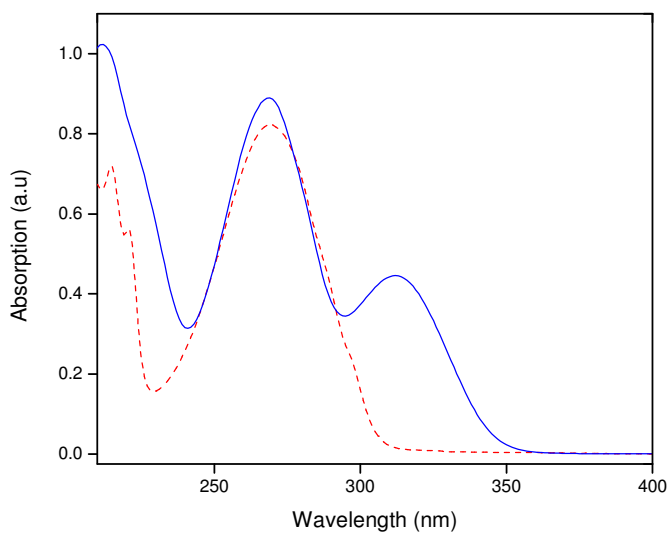
Figure S1: Representative UV spectra collected during the release of Cn (– – –) and o-HCn (—).
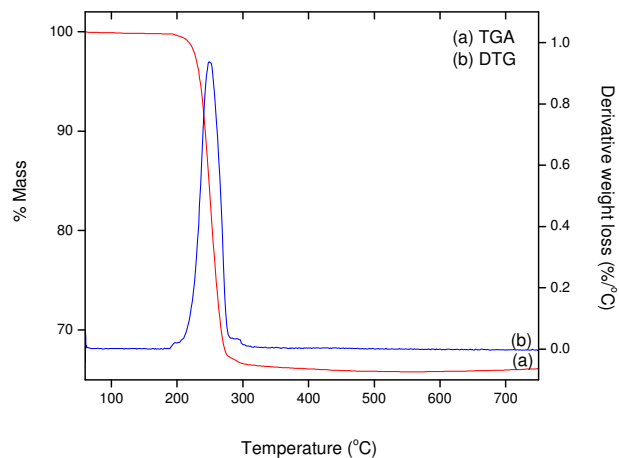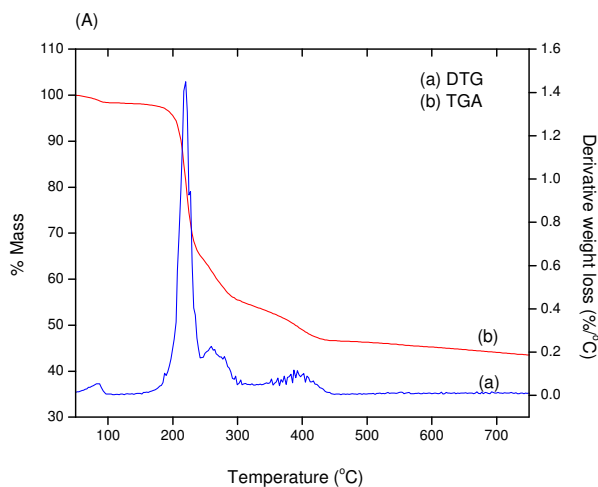
Figure S2: TG (b) and DTG (a) curves for (A) C-*o*-HCn and (B) BCN, in nitrogen atmosphere at a ramp rate of 20°/min.
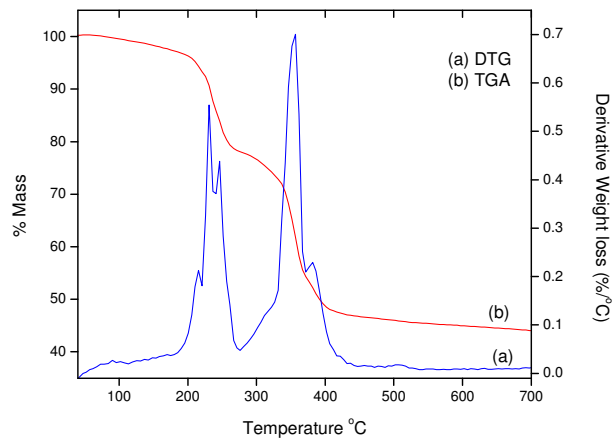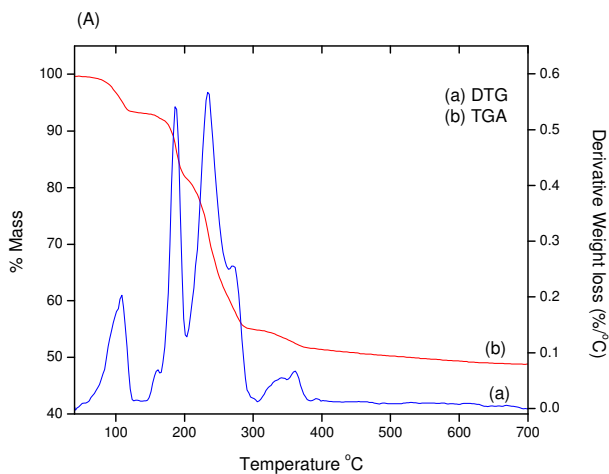
Figure S3: TG (b) and DTG (a) curves for (A) ZC-Ac and (B) ZC-Cn, in nitrogen atmosphere at a ramp rate of 20°/min.
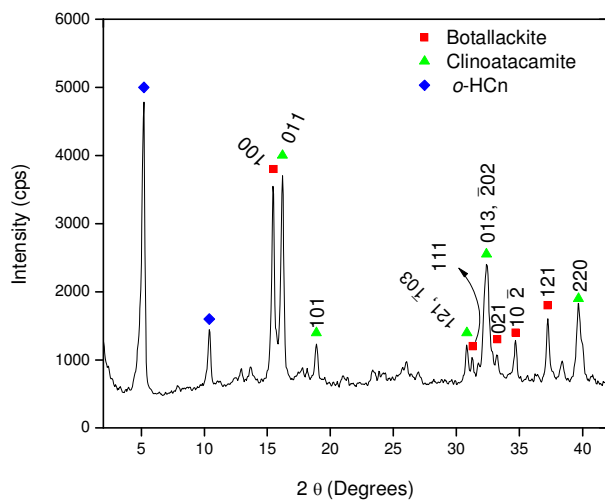
Figure S4: XRD profile of C-o-HCn exchanged with chloride for 60 minutes at 60°C. O-HCn phase is represented by closed diamonds, botallackite phase by closed squares [PDF# 58-520] and clinoatacamite phase by closed triangles [PDF# 50-1559].
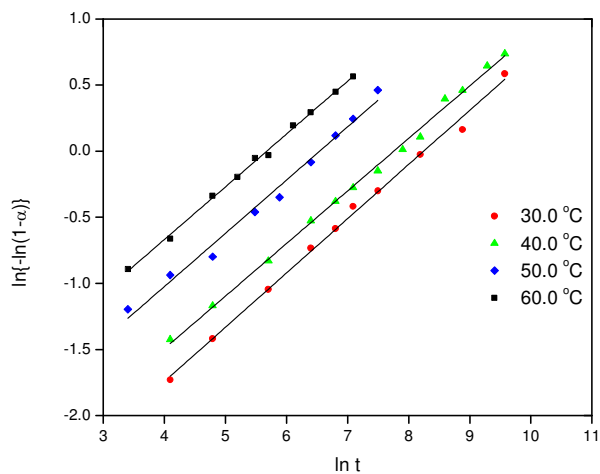

Figure S5: Double-logarithmic plots for the exchange reaction of Cl⁻ anion and C-o-HCn at various temperatures for solution analysis: 60°C (■), 50°C (♦), 40 °C (▲), 30°C (●).
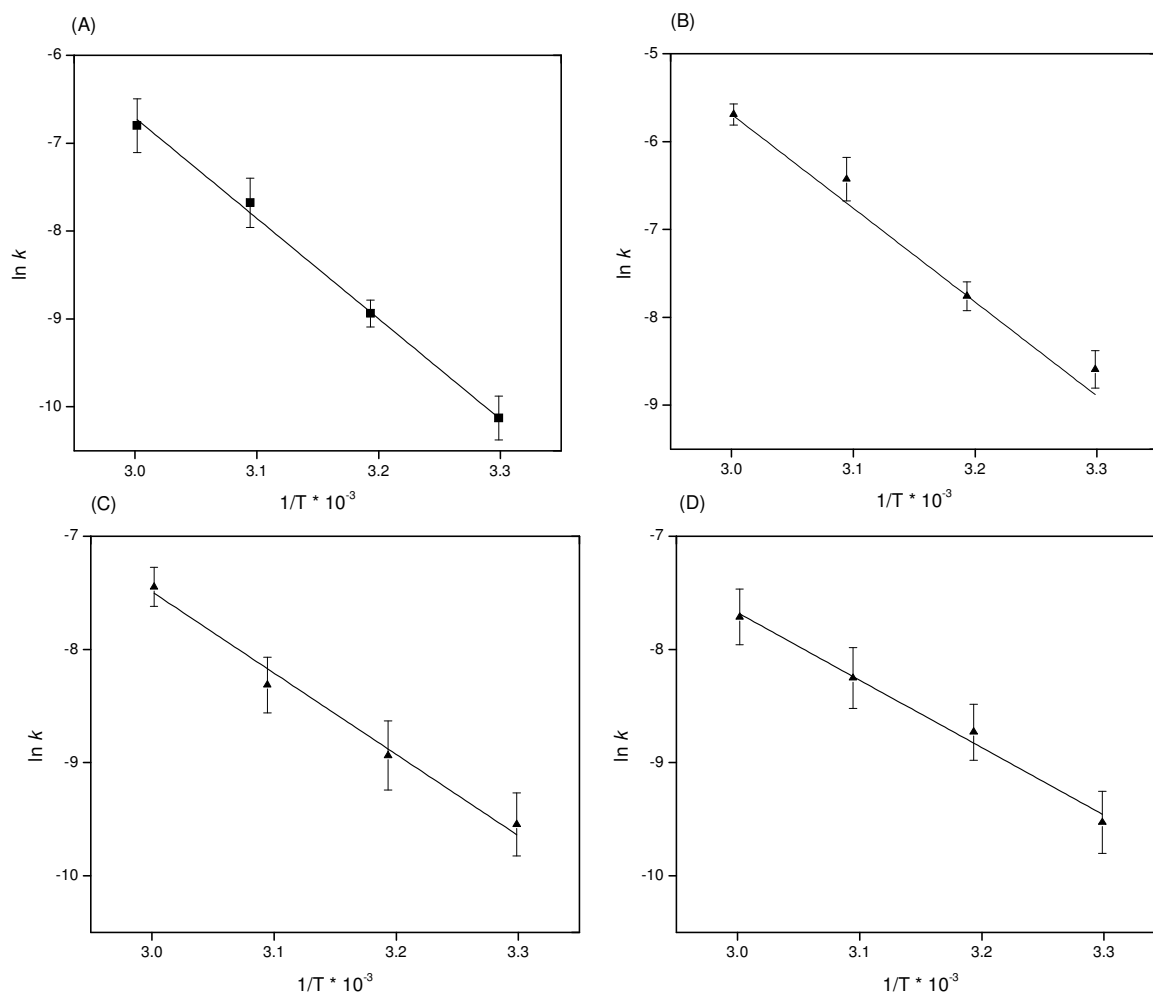
Figure S6. Arrhenius plots for the determination of the activation energy for (I) the release of o-HCn from C-*o*-HCn for (A) solid state analysis, (B) solution analysis and (II) for the release of Cn from ZC-Cn (C) solid state analysis and (D) solution analysis
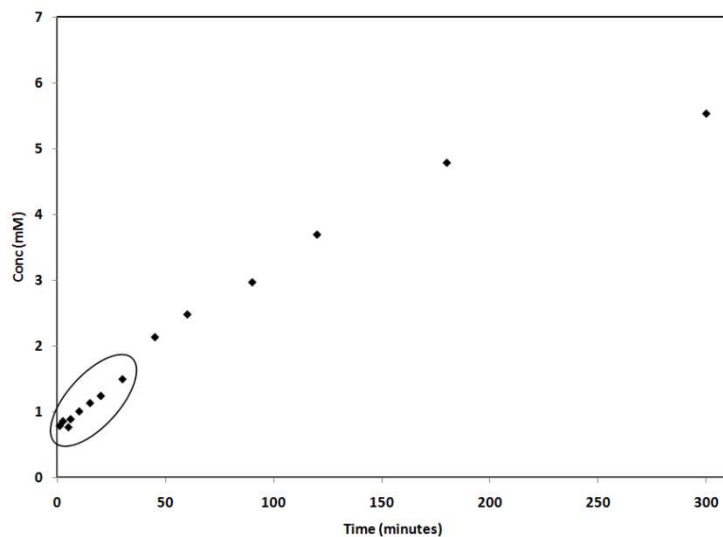
Figure S7. Released [Cn] as a function of time highlighting the period of slow and linear accumulation of Cn anions.
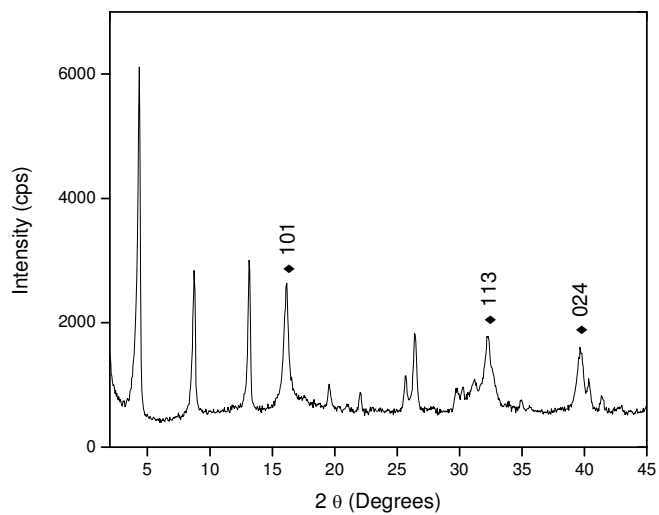

Figure S8: XRD profile of ZC-Cn exchanged with chloride for 60 minutes at 50°C. Chloride phase has been indexed as paratacamite represented by closed triangles [PDF# 50-1558].
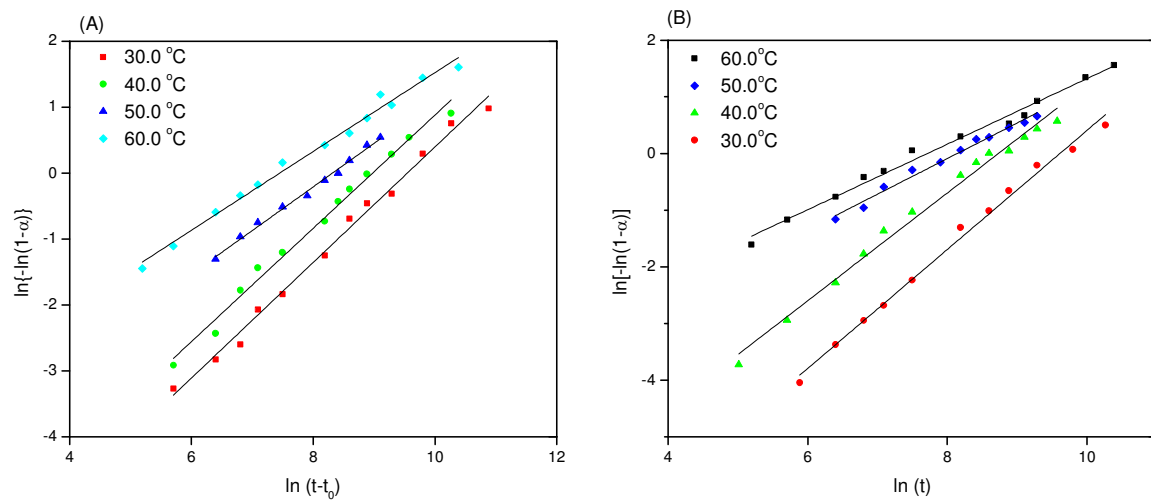
Figure S9: Double-logarithmic plots for the exchange reaction of Cl⁻ anion and ZC-Cn at various temperatures for A) solid state analysis and (B) solution analysis: 60°C (■), 50°C (♦), 40 °C (▲), 30°C (●).